


Cite this: *Chem. Commun.*, 2019, 55, 10756Received 28th May 2019,
Accepted 10th July 2019

DOI: 10.1039/c9cc04102h

rsc.li/chemcomm

Synthesis of supramolecular gels based on electron-transfer reactions between clay nanotubes and styrene†

Jingqi Zheng, Xianfeng Ou, Fan Wu and Mingxian Liu *

A novel supramolecular gel is synthesized using styrene and halloysite nanotubes under ultrasound treatment, in which the nanotubes act as gelators for the styrene gel. The formation of the gel arises from electron-transfer reactions between styrene and the aluminium atoms at the crystal edges and the transition metal ions of the clay. The supramolecular gel is transparent and sensitive to temperature, which shows promising applications in sensors, templates, and gelling fuels.

Halloysite nanotubes (HNTs) are a kind of clay mineral. The chemical formula of HNTs is $\text{Al}_2\text{Si}_2\text{O}_5(\text{OH})_4 \cdot n\text{H}_2\text{O}$ which is similar to that of kaolin.¹ Microscopically, HNTs have a hollow tubular structure with a length of 200–1500 nm and an outer diameter of about 50 nm.² The application of HNTs in various fields is based on their particular tubular structure. Generally, HNTs show high reinforcing ability towards polymers and a good dispersion state.³ In the biomedical field, HNTs are applied to fabricate tissue engineering scaffolds as well as drug delivery systems, and also serve as gene transfection vectors.⁴ Additionally, HNTs undergo self-assembly during their aqueous solution drying, which will form special patterns for capturing cells or directing the growth of stem cells.^{5,6} HNTs are also widely used in the field of sewage treatment, catalysts, electrolytes for lithium batteries, and so on.^{7,8}

Clay minerals have been involved in the abiotic origin of life on Earth as a consequence of their ability to adsorb, protect, concentrate, and transform biomolecules.⁹ Clay minerals react with different types of organic compounds in particular ways. Generally, there are three kinds of interactions between clay minerals and organic molecules, including adsorption, intercalation and cation exchange.¹⁰ For example, kaolin can adsorb particular types of organic compounds on its surfaces.

Montmorillonite can be intercalated by various organic molecules into the interlayer space. The intercalation of guest molecules can be used for the preparation of polymer composites. Solomon *et al.* found that certain clay minerals (attapulgite and montmorillonite) can act as catalysts in polymerization of unsaturated organic compounds such as styrene (St) and hydroxyethyl methacrylate.¹¹ This process is related to a charge transfer reaction between clay minerals and organic molecules. Clay minerals provide sufficient electron accepting sites while organic molecules donate electrons, which is evident in the polymerization of organic matter. The electron accepting sites are aluminium atoms and transition metals (such as ferric ions) in the higher valence state at the edge of the clay mineral crystal.¹² Under certain conditions, the organic substance is active to undergo polymerization after electron transfer, as shown in Fig. 1A. Here, we report another electron transfer reaction between St and HNTs and the phenomenon of formation of a stable supramolecular gel under ultrasound

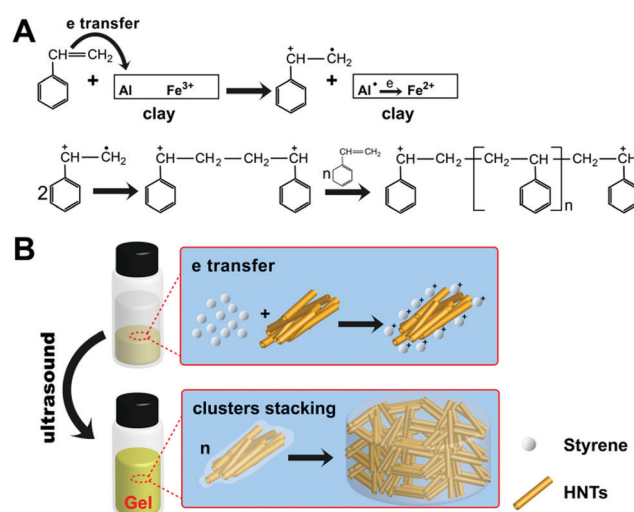


Fig. 1 The electron transfer mechanism of St and clay (A) and the schematic showing the formation of the St@HNT supramolecular gel by electron transfer interactions (B).

Department of Materials Science and Engineering, Jinan University, Guangzhou, Guangdong 510632, P. R. China. E-mail: liumx@jnu.edu.cn; Fax: +86 20-85223271; Tel: +86 20-85226663

† Electronic supplementary information (ESI) available. See DOI: 10.1039/c9cc04102h

treatment. Pure HNT hydrogel can be formed at a concentration of nanotubes higher than 40 wt% in aqueous solution.¹³ No HNT organic gel has been reported until now.

In the St and HNT gel, HNTs play a role as gelators. In comparison to kaolin, HNTs are easy to disperse and easily provide more crystal edges due to their tubular morphology. Free electrons derived from the conjugated structure of St can be transferred to aluminium atoms and ferric ions on the crystal edges of HNTs. The polycations of St molecules are then adsorbed on HNTs by electrostatic interaction which is generated between the cationic groups of the pre-polymer and the negatively charged surfaces of HNTs.¹⁴ When numerous St polycations are adsorbed on HNTs, a gel-like layer of St is formed around the nanotubes. Raw HNT powder is microscopically agglomerated nanotubes. Upon addition of HNTs to St, large agglomerates are broken into small clusters under the ultrasound effect. Clusters composed of several nanotubes are homogeneously distributed in the St medium *via* strong electrostatic interaction. Hence, a styrene@halloysite nanotube (St@HNT) supramolecular gel is formed when a sufficient amount of HNT powder is mixed with the St solvent (Fig. 1B). The samples were characterized by zeta potential testing and the dynamic light scattering (DLS) method. As shown in Fig. S1A (ESI[†]), the absolute value of the zeta potentials of St@HNTs decreases compared with those of raw HNTs. For example, the zeta potentials of St@HNTs 100-10 and St@HNTs 100-20 are -20.7 mV and -20.3 mV respectively, while that of raw HNTs is -25.2 mV. At the same concentration of water dispersions, the particle size distribution of HNTs is obviously smaller than that of St@HNTs (Fig. S1B–F, ESI[†]). These results suggest that the surfaces of HNTs are covered by positively charged St polycations *via* electrostatic interaction. In addition, St@HNTs 100-20 was characterized by electron paramagnetic resonance (EPR). As shown in Fig. S2 (ESI[†]), a signal can be obtained, which indicates that there are free radicals in this system. This confirms the mechanism of free radical formation *via* electron transfer. However, the signal is not easy to detect because the concentration of free radicals is low in comparison to the polymerization of St using an organic initiator.^{15,16}

As shown in Fig. 2A, the appearance of St is clear and transparent. As the amount of HNTs increases, the transparency of the mixture slightly decreases. After St and HNTs are evenly mixed under ultrasound treatment, HNTs would sink to the

bottom under the action of gravity. At a concentration of HNTs higher than 90.9 mg mL⁻¹, the mixture of St and HNTs begins to show a gel state. The gel does not flow even upon inverting the bottle. The appearance of St@HNTs 100-20 is light yellowish green with a certain light transmission. After a large amount of HNTs is added for example 272.7 mg mL⁻¹, the mixture becomes a yellow gel without transparency. However, St and other clay minerals such as attapulgite, montmorillonite and kaolin are mixed in the same manner and ratio, but the appearances of these mixtures are unlike that of St@HNTs 100-20 (Fig. S3A–C, ESI[†]). The curled crystal structures of HNTs provide a greater number of charge transfer sites than those of other types of clay minerals.^{16,17} Thus, a small number of HNTs would interact with St and they will form a uniform gel. After the crystal edges of HNTs are masked by sodium tripoly phosphate, the electron accepting properties of the crystal edges of HNTs are lost, and thus the mixture of St and HNTs shows fluidity (Fig. S3D, ESI[†]).

HNTs have a high aspect ratio, which could form an ordered arrangement to display the polarization phenomenon.^{18,19} St@HNTs were characterized by polarized optical microscopy (POM) to observe the distribution of HNTs in the St medium. Aggregates with yellow and blue color shown in Fig. 2B and Fig. S4 (ESI[†]) illustrate that HNTs present a partially dispersed state in St rather than tube dispersion on the nanoscale, which is the reason for the generated birefringence observed under POM.¹³ With the increase of HNT content, the number and size of the aggregates increase. In the same observation area, when the rotation angle is 180° , the color of HNT aggregates is the same as that in the POM images, as shown in Fig. S5 (ESI[†]). The color of aggregates changes when the rotation angle of the observed sample is less or more than 180° . The rheological properties of St@HNTs 100-20 and St@HNTs 100-5 are shown in Fig. S6 (ESI[†]). In comparison to St@HNTs 100-5 which is in liquid state, the viscosity of St@HNTs 100-20 is larger. St@HNTs 100-20 shows a shear thinning behaviour due to the breaking of the HNT network as shown in Fig. S6B (ESI[†]). In the linear viscoelastic region of St@HNTs 100-20 (Fig. S6C, ESI[†]), the critical stress is 53.8 Pa. After exceeding the critical stress, the storage modulus of St@HNTs 100-20 begins to decline.

The dispersion state of HNTs in St was characterized by TEM and SEM. In the diluted dispersion, it is easy for HNTs to form ring-like agglomerates in St, as shown in Fig. 3A and Fig. S7 (ESI[†]). However, at the same concentration of the aqueous dispersion of HNTs, single tubes and bundles are randomly distributed as shown in Fig. 3B. The surface of raw HNTs has hydrophilic groups and exhibits excellent dispersibility in aqueous solution. The stability of HNT dispersion in water is due to the surface of HNTs with a highly negative charge.¹³ The stability of the gel arises from the network structure formed by nanotubes. Fig. 3C shows the morphology of HNTs in St@HNTs 100-20 which is dried at room temperature and St is volatilized completely. It is clear that HNTs are stacked in a cluster state with certain alignment, and there are certain gaps between the HNT clusters (corresponding to the St location). The dry skeleton of nanotubes forms a certain ordered structure. In the gel, St is fixed in the spacing among the ordered nanotubes. This result is consistent

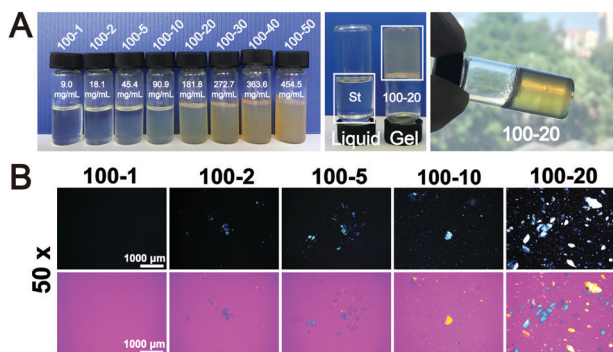


Fig. 2 The appearance of St@HNTs (A) and polarized optical micrograph of St@HNTs (B).

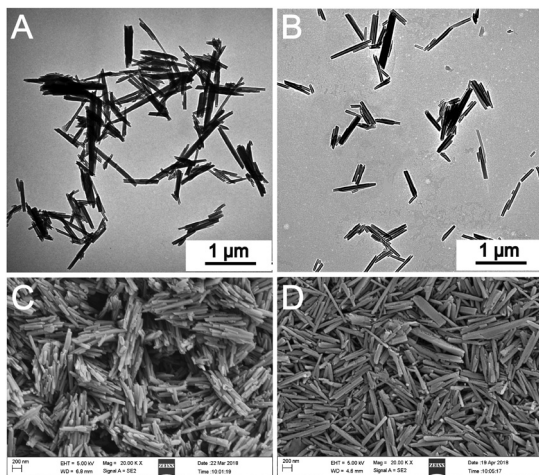


Fig. 3 TEM image of HNTs dispersed in the St solvent (A) and in water (B); SEM image of the St@HNT gel (100-20) (C) and 20 wt% water dispersion solution of HNTs (D).

with the POM result. HNTs were also dispersed in water in the same ratio to prepare a control sample and the water in the sample was also evaporated at room temperature. This shows that HNTs are randomly dispersed and stacked to form a relatively flat surface, as shown in Fig. 3D. This also indicates that the interaction between St and HNTs is different from that between water and HNTs.

For investigating the preparation conditions for the formation of the St@HNT gel, different ultrasound time was employed to synthesize St@HNTs 100-20. Fig. S8 (ESI[†]) reveals that the macroscopic stability of the gel increases when the ultrasound time increases. Under ultrasound treatment, HNT aggregates can be broken in the St medium. It is apparent that the large agglomerates become smaller as the ultrasound time increases. The longer the ultrasound time is, the more uniform the dispersion of the nanotubes is. The interface area between St and HNTs is enhanced by the formation of HNT clusters. This proves that the ultrasound treatment is the driving force for HNTs to be dispersed in the St medium. The interaction between HNT clusters and St is the key for the formation of the gel. The thermal stability of St@HNTs has also been studied (Fig. S9, ESI[†]). As we know, the melting point of St is $-30.6\text{ }^{\circ}\text{C}$. At $-80\text{ }^{\circ}\text{C}$, St in the gel is frozen. When the frozen gel is kept at room temperature again, the frozen solvent quickly liquefies and solid-liquid separation of HNTs and St in the gel occurs. With ultrasound treatment again, the phase-separated St@HNT mixture would form a stable gel again. After storing at $-20\text{ }^{\circ}\text{C}$, $60\text{ }^{\circ}\text{C}$ and $80\text{ }^{\circ}\text{C}$ for 24 h, St@HNTs 100-20 still remains stable. Generally, St is polymerized under heat treatment. Thus, after being treated at $60\text{ }^{\circ}\text{C}$ for 14 days, the gel (St@HNTs 100-20) becomes a viscous fluid which demonstrates that a certain degree of polymerization of St in the gel has occurred. Fig. S10 (ESI[†]) proves that HNTs in the gel are further uniformly dispersed in St during the polymerization of St which is initiated by the thermal effect. By further extending the heat treatment time, the HNTs@polystyrene (HNTs@PS) composite was finally obtained and its cross section was observed by SEM

(Fig. S11, ESI[†]). Markedly, the clusters of HNTs are immobilized in the PS matrix. HNTs in each cluster have a preferred alignment, while HNT clusters are randomly distributed in the PS matrix, which is consistent with the SEM images of the HNT skeleton of St@HNTs 100-20.

The interaction between St and HNTs is further investigated. The FTIR spectra of St, St@HNTs 100-20 and HNTs are shown in Fig. S12A (ESI[†]). The peaks of St from 3094 to 2977 cm^{-1} are attributed to the C-H bonds on the benzene ring and the peaks near 1496 cm^{-1} are assigned to the vibrations of the benzene ring.²⁰ The peak at 685 cm^{-1} is related to a single substitution of the vinyl group on the phenyl ring. The peaks of HNTs that appeared at 3699 and 3619 cm^{-1} are attributed to the stretching vibrations of O-H groups.²¹ Obviously, the FTIR spectrum of St@HNTs 100-20 contains characteristic peaks of both St and HNTs, but no new peak appears which indicates that there is no chemical bonding between St and HNTs. The standard IR spectrum of PS is used for comparison, which clearly shows that St in the gel is mostly like the St monomer. This indicates that polycations undergo a small degree of polymerization at the beginning. As shown in Fig. S12B (ESI[†]), the crystal structures of HNTs in the gel and HNTs in the dry gel are consistent with the crystal structure of HNTs. No intercalating effect of St or PS towards HNTs has been identified since the layer spacing of the (001) plane is still maintained at 7.0 \AA . It is further proved that the interaction between St and HNTs is physical rather than chemical. It can be seen from the UV-vis spectrum (Fig. 4) that the St@HNTs samples at different ratios are consistent in the $n \rightarrow \pi^*$ absorption band (281.6 nm) of St, but the B absorption band (290.3 nm) is slightly different. This indicates that the $\pi \rightarrow \pi^*$ transition of the carbon atom in the benzene ring on St is influenced by HNTs. The excellent physical adsorption capacity of HNTs towards organics is related to their special microstructure. Interactions between St and HNTs are more than physical adsorption. There is no gelation between other organic solvents (such as cyclohexane) and HNTs under ultrasound treatment. So, it is considered that a supramolecular St@HNT gel is obtained *via* the electron transfer interactions. The preparation method is also effective to form an α -methyl styrene@HNT gel (Fig. S13A, ESI[†]).

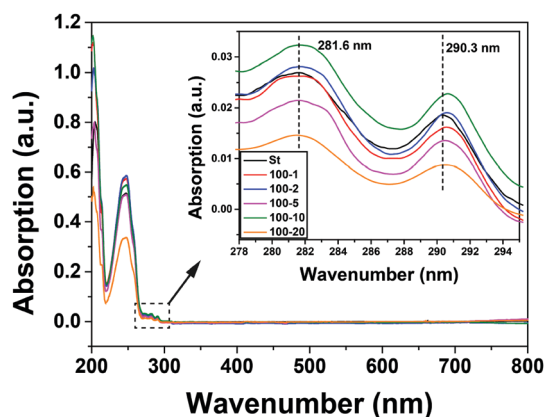


Fig. 4 UV-vis spectrum of St@HNTs.

Ethyl benzene was also mixed with HNTs (181.8 mg mL^{-1}). As shown in Fig. S13B (ESI[†]), HNTs have a good compatibility with ethyl benzene. However, their appearance is unlike that of St@HNTs and α -methyl styrene@HNTs at the same concentration, which appears white without transparency. Their zeta potential shows a small difference from that of St@HNTs 100-20 (Fig. S13C, ESI[†]). These organic molecules all have a conjugated structure, but their degree of conjugation with ethyl benzene is smaller than that with styrene and α -methyl styrene.

In summary, a supramolecular gel composed of St and HNTs is prepared under ultrasound treatment. The mechanism of gel formation is ascribed to the electron-transfer reaction. Electrons on the conjugated St molecule are transferred to the clay surfaces through the electron accepting sites of aluminium atoms and Fe^{3+} ions in HNTs. HNTs play a role as gelators of the supramolecular gel while the polycations of St are adsorbed in the HNT skeleton. The results of the morphology and the UV-vis spectrum prove the interaction mechanism. The prepared St@HNT gels have promising applications in sensors, templates, and gelling fuels.

This work was financially supported by the National Natural Science Foundation of China (51473069 and 51502113), the Pearl River S&T Nova Program of Guangzhou (201610010026), and the Fundamental Research Funds for the Central Universities (21619102).

Conflicts of interest

There are no conflicts to declare.

Notes and references

- 1 M. Liu, Z. Jia, D. Jia and C. Zhou, *Prog. Polym. Sci.*, 2014, **39**, 1498–1525.
- 2 Y. Lvov, W. Wang, L. Zhang and R. Fakhruddin, *Adv. Mater.*, 2016, **28**, 1227–1250.
- 3 P. Yuan, D. Tan and F. Annabi-Bergaya, *Appl. Clay Sci.*, 2015, **112–113**, 75–93.
- 4 A. C. Santos, C. Ferreira, F. Veiga, A. J. Ribeiro, A. Panchal, Y. Lvov and A. Agarwal, *Adv. Colloid Interface Sci.*, 2018, **257**, 58–70.
- 5 M. Liu, Z. Huo, T. Liu, Y. Shen, R. He and C. Zhou, *Langmuir*, 2016, **33**, 3088–3098.
- 6 X. Zhao, C. Zhou, Y. Lvov and M. Liu, *Small*, 2019, **15**, 1900357.
- 7 V. A. Vinokurov, A. V. Stavitskaya, A. P. Glotov, A. A. Novikov and Y. M. Lvov, *Chem. Rec.*, 2018, **18**, 858–867.
- 8 L. Yue, X. Wang, L. Jin and J. D. Miller, *Nano Energy*, 2017, **31**, 478–485.
- 9 C. Ponnampuruma, A. Shimoyama and E. Friebele, *Origins Life*, 1982, **12**, 9–40.
- 10 G. Lagaly, *Clay-organic interactions*, University School of Chemical Sciences, Dublin City, 1988, vol. 311, pp. 75–117.
- 11 D. H. Solomon, *Clays Clay Miner.*, 1968, **16**, 31–39.
- 12 D. H. Solomon, *Clay Miner.*, 1968, **7**, 399–408.
- 13 Z. Luo, H. Song, X. Feng, M. Run, H. Cui, L. Wu, J. Gao and Z. Wang, *Langmuir*, 2013, **29**, 12358–12366.
- 14 B. K. G. Theng, *Clays Clay Miner.*, 1982, **30**, 1–10.
- 15 B. Yamadaa, D. G. Westmorelandb, S. Kobatakea and O. Konosu, *Prog. Polym. Sci.*, 1999, **24**, 565–630.
- 16 D. H. Solomon and M. J. Rosser, *J. Appl. Polym. Sci.*, 1965, **9**, 1261–1271.
- 17 Y. Zhao, E. Abdullayev, A. Vasiliev and Y. Lvov, *J. Colloid Interface Sci.*, 2013, **406**, 121–129.
- 18 Z. Luo, A. Wang, C. Wang, W. Qin, N. Zhao, H. Song and J. Gao, *J. Mater. Chem. A*, 2014, **2**, 7327.
- 19 M. Liu, R. He, J. Yang, W. Zhao and C. Zhou, *ACS Appl. Mater. Interfaces*, 2016, **8**, 7709–7719.
- 20 B. J. Kim and K. S. Kang, *Synth. Met.*, 2013, **169**, 55–58.
- 21 J. Madejová, *Vib. Spectrosc.*, 2003, **31**, 1–10.

Electronic Supplementary Information

Synthesis of supramolecular gels based on electron-transfer reactions between clay nanotubes and styrene

*Jingqi Zheng, Xianfeng Ou, Fan Wu, Mingxian Liu**

Department of Materials Science and Engineering, Jinan University, Guangzhou
510632, People's Republic of China

*Corresponding author. Tel.: (86)20-85226663. Fax: (86)20-85223271.

E-mail: liumx@jnu.edu.cn

Experimental details:

1. Materials

Halloysite nanotubes (HNTs) were purchased from Guangzhou Runwo Materials Technology Co., Ltd., China. HNTs were purified according to the reference to remove the impurities.¹ Styrene (St) was obtained from Tianjin Damao Chemical Reagent Co., Ltd, China. Other chemicals used in the experiment were supplied by Aladdin Industrial Co., China.

2. Sample preparation

HNTs were added to St and they were mixed by shaking. Then, the mixture was placed in an ultrasonic cleaner for sonication for a certain time to obtain gel. Mixture of St and HNTs was denoted as St@HNTs with St and HNTs weight ratio. For example, St@HNTs 100-20 meant the weight ratio between St and HNTs was 100: 20. St@HNTs meant 5 kinds of mixtures: St@HNTs 100-1, St@HNTs 100-2, St@HNTs 100-5, St@HNTs 100-10 and St@HNTs 100-20. Additionally, α -methyl styrene@HNTs and ethyl benzene@HNTs were prepared with a weight ratio between corresponding organic substance and HNTs was 100: 20.

HNTs masked by sodium tripoly phosphate were prepared as follows. HNTs and sodium tripoly phosphate were added in ultrapure water in proportion of 0.05 mol sodium tripoly phosphate per 100 g HNTs. The suspension was stirred for 6 h. Then, HNTs in the suspension were centrifuged and washed three times with ultrapure water. After drying under 60°C, HNTs masked by sodium tripoly phosphate were obtained.

3. Characterization

Zeta potential. The samples were diluted to 0.5 wt% aqueous suspensions for testing, which were tested by a Nano ZS zeta-potential analyzer (Malvern Instruments Co., U.K.).

Dynamic light scattering (DLS). The samples were prepared by diluting HNTs or St@HNTs to 0.045wt% suspension with ultrapure water, which were tested by a nanoparticle size and zeta potential analyzer (Omni, Brookhaven Instruments Co., USA).

Electron paramagnetic resonance (EPR). The test method of EPR test was based on the relevant literature.² St (300 μ L) and HNTs (54 mg) were placed in a Pyrex EPR tube (i.d. 3.8 mm). The solution in tube was degassed through repeated freeze and thaw cycles. Then, the tube was saturated with argon. After being sealed, it was placed in the cavity of the EPR spectrometer (JES FA300, JEOL Ltd., Japan) to test. Spectra were recorded repeatedly until the spectral pattern showed no further change.

Polarized optical microscopy (POM). St@HNTs gels were coated to a glass slide and covered with another piece of glass to get the samples which were observed under a polarized optical microscope (BX51, Olympus, Japan).

The rheological behavior. The dynamic viscosity was measured by a hybrid rheometer (TA Discovery HR-2, USA) using a parallel plate model with a diameter of 40 mm at 25°C. The shear rate of the shear stress and the dynamic viscosity was from 10^{-1} s^{-1} to

10^2 s^{-1} . The strain scan range of St@HNTs 100-20 was from $10^{-4}\%$ to $10^3\%$.

Transmission electron microscopy (TEM). The HNT dispersion (in St solvent or ultrapure water) was dropped on carbon film supported by a copper grid. After evaporation of the solvent, the samples were characterized by TEM (JEM-2100F, JEOL Ltd., Japan).

Scanning electron microscopy (SEM). St@HNTs 100-20 and water dispersion of HNTs (20 wt%) were coated on the glass and the solvent were fully volatilized. The images were taken through SEM (Ultra-55, Carl Zeiss Jena Ltd., Germany) with an accelerating voltage of 5 kV. The cross sections of HNTs@polystyrene (HNTs@PS) to be observed were obtained after being broken in liquid nitrogen.

Fourier transform infrared spectroscopy (FTIR). The FTIR spectra were characterized by a Thermo FTIR (Nicolet iS50, Thermo Fisher Scientific Ltd., USA). The wavenumber ranged from 4000 cm^{-1} to 500 cm^{-1} .

X-ray diffraction (XRD). The XRD patterns were recorded through an X-ray diffractometer (MiniFlex-600, Rigaku Co., Japan). The scanning angle was from 5° to 60° while the scanning speed was $5^\circ/\text{min}$.

UV-vis spectrum. St@HNTs gel was diluted to 500 ppm with alcohol and scanned in 200-800 nm by an ultraviolet spectrophotometer (UV-2550, Shimadzu Instrument Ltd., Japan).

Supporting figures:

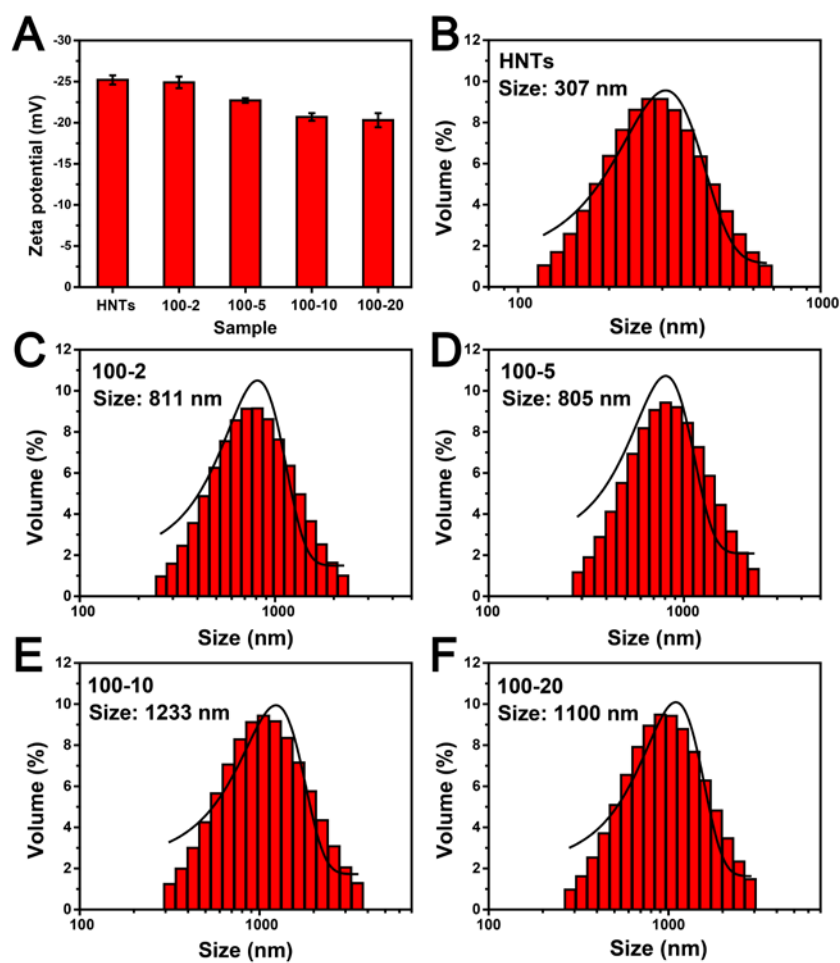


Fig. S1 Zeta potential of HNTs and St@HNTs (A); DLS results of HNTs and St@HNTs (B: HNTs; C: St@HNTs 100-2; D: St@HNTs 100-5; E: St@HNTs 100-10; F: St@HNTs 100-20).

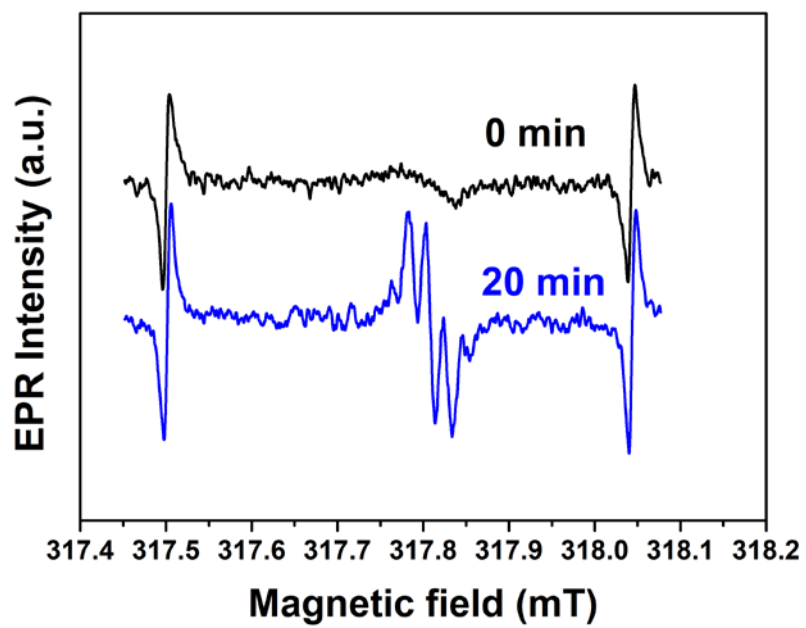


Fig. S2 EPR curves of St@HNTs 100-20 at different time.

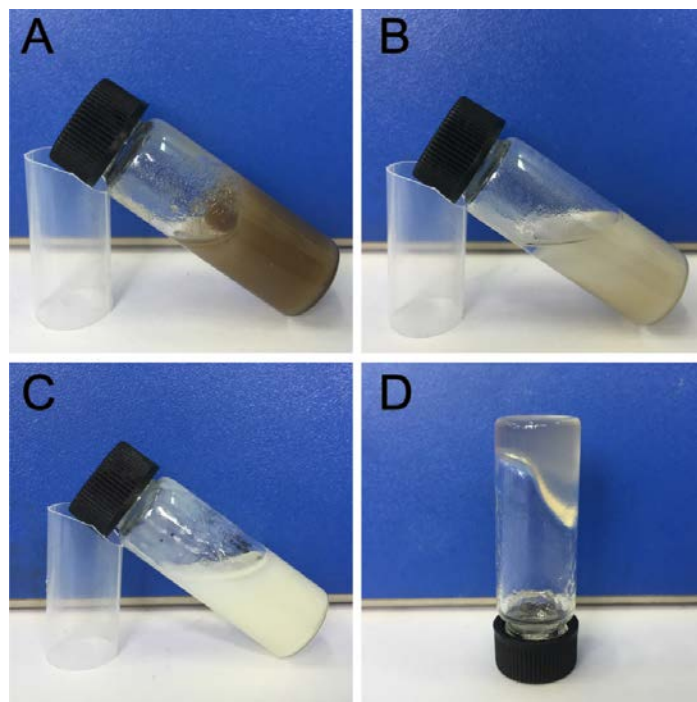


Fig. S3 The appearance of mixture of St and clay minerals with ultrasound treatment for 30 min (A: attapulgite; B: montmorillonite; C: kaolin; D: HNTs masked by the polyphosphate).

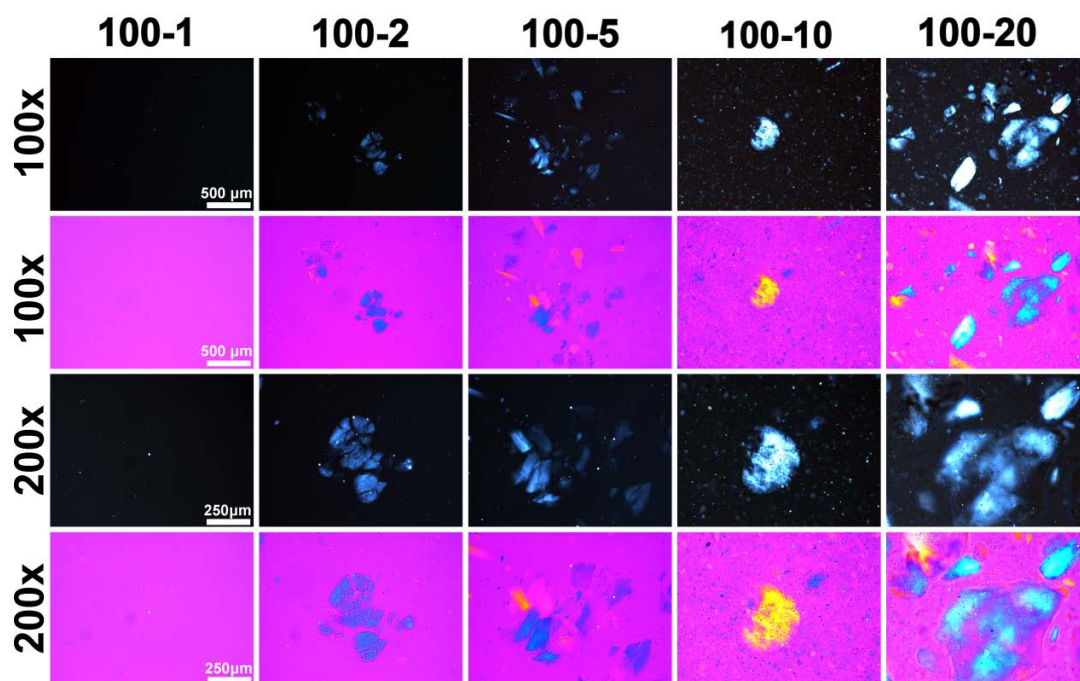


Fig. S4 Polarized optical micrograph of St@HNTs with different magnification.

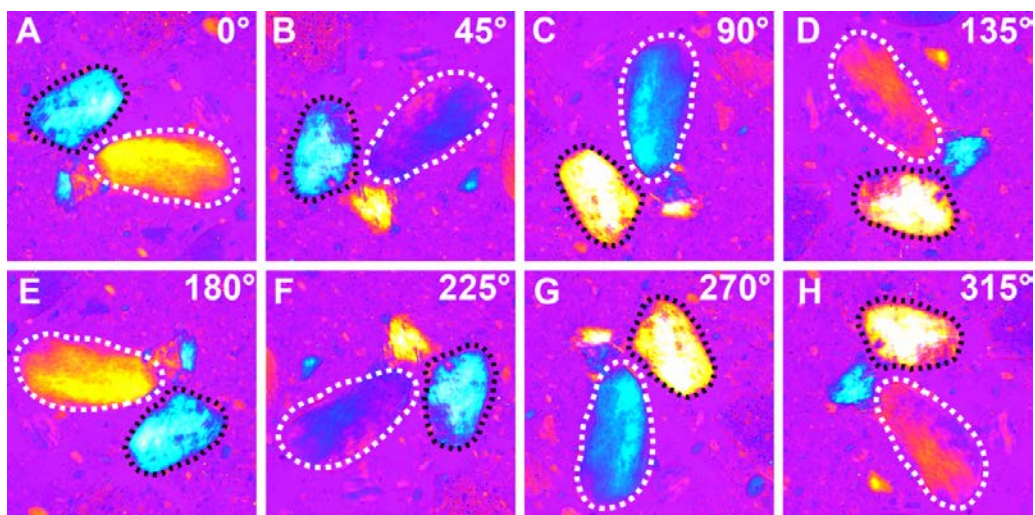


Fig. S5 Polarized optical micrograph of St@HNTs 100-20 in the same area by rotating different angle.

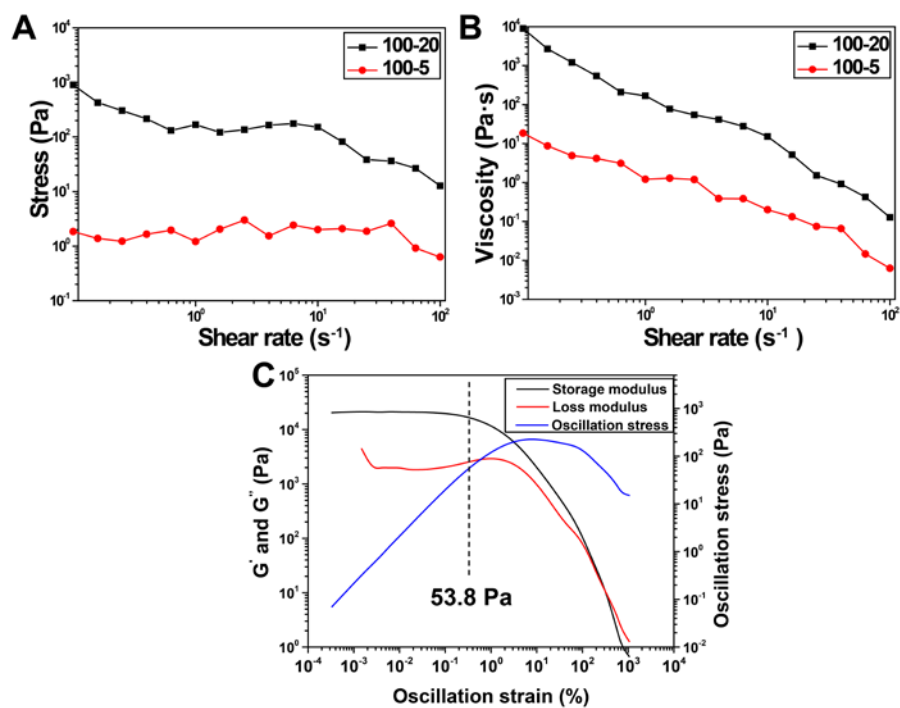


Fig. S6 Shear stress vs shear rate curves (A) and shear viscosity vs shear rate curves (B) of St@HNTs gel (St@HNTs 100-20 and St@HNTs 100-5); strain scanning curves (C) of St@HNTs 100-20.

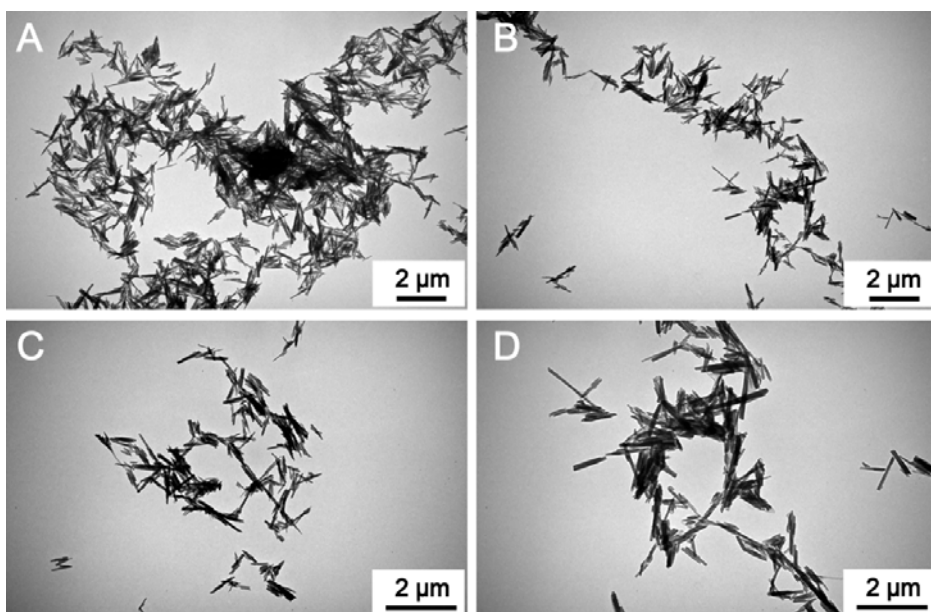


Fig. S7 TEM image of HNTs dispersed in St with different magnification.

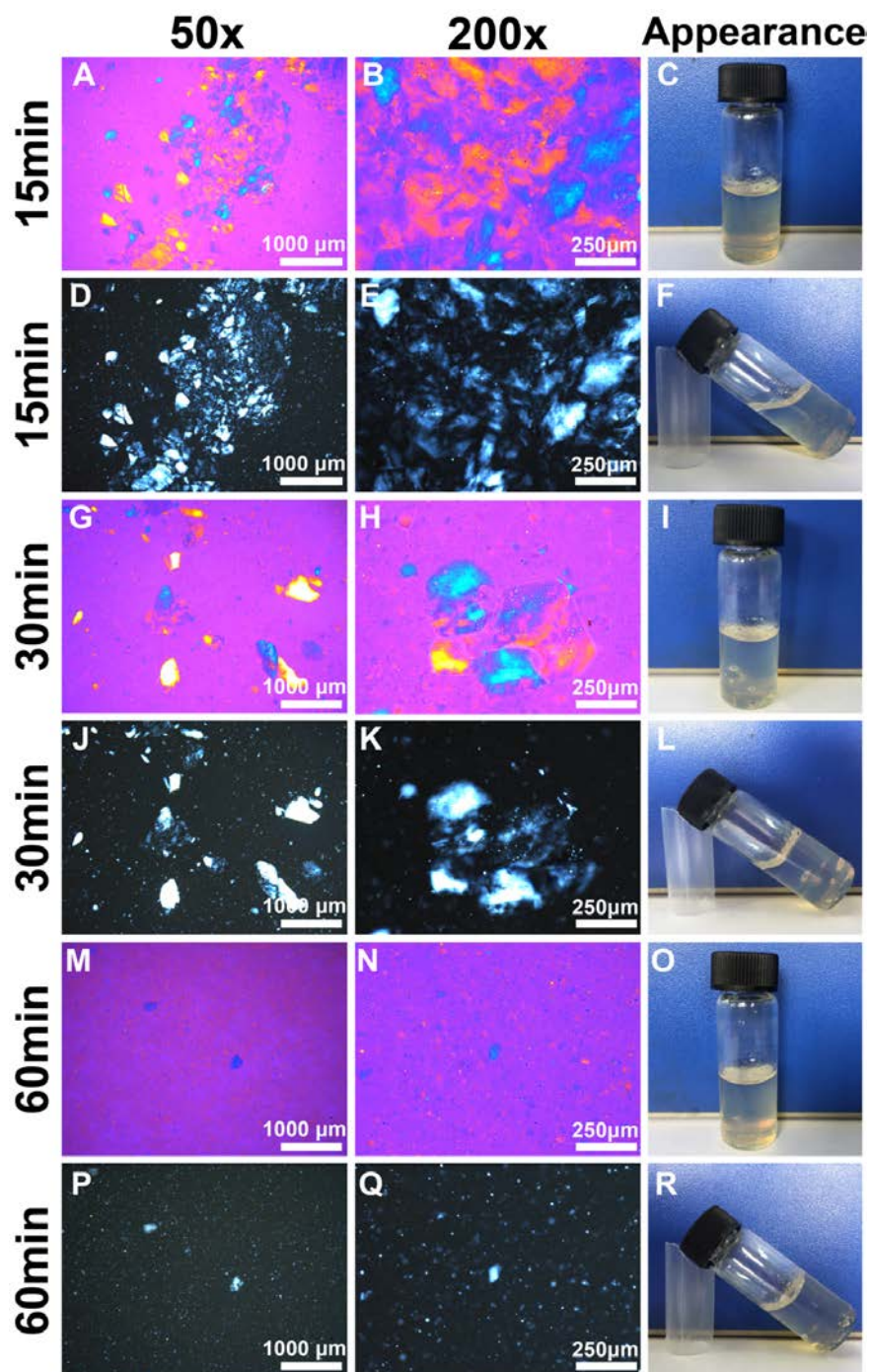


Fig. S8 Effect of ultrasonic time on St@HNTs 100-20 (15 min: A, B, C, D, E, F; 30 min: G, H, I, J, K, L; 60 min: M, N, O, P, Q, R).

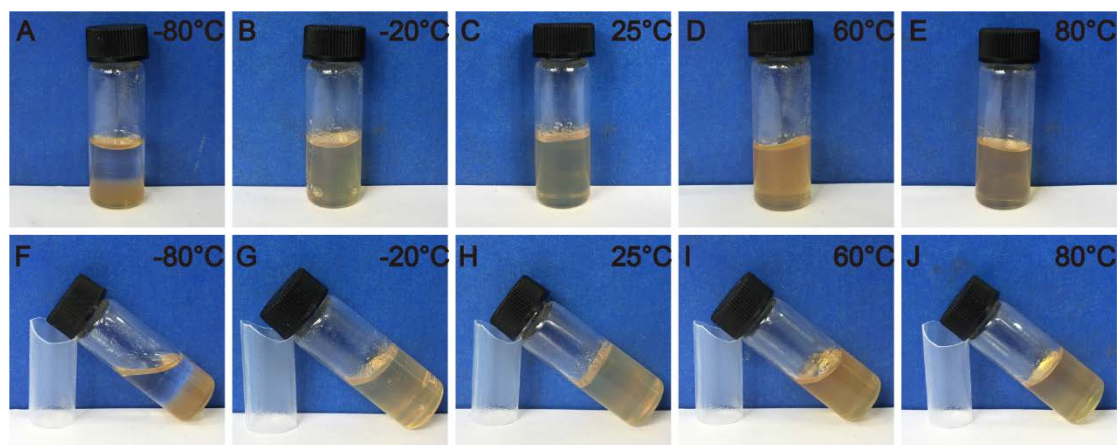


Fig. S9 Effect of temperature on St@HNTs 100-20 (-80°C: A, F; -20°C: B, G; 25°C: C, H; 60°C: D, I; 80°C: E, J).

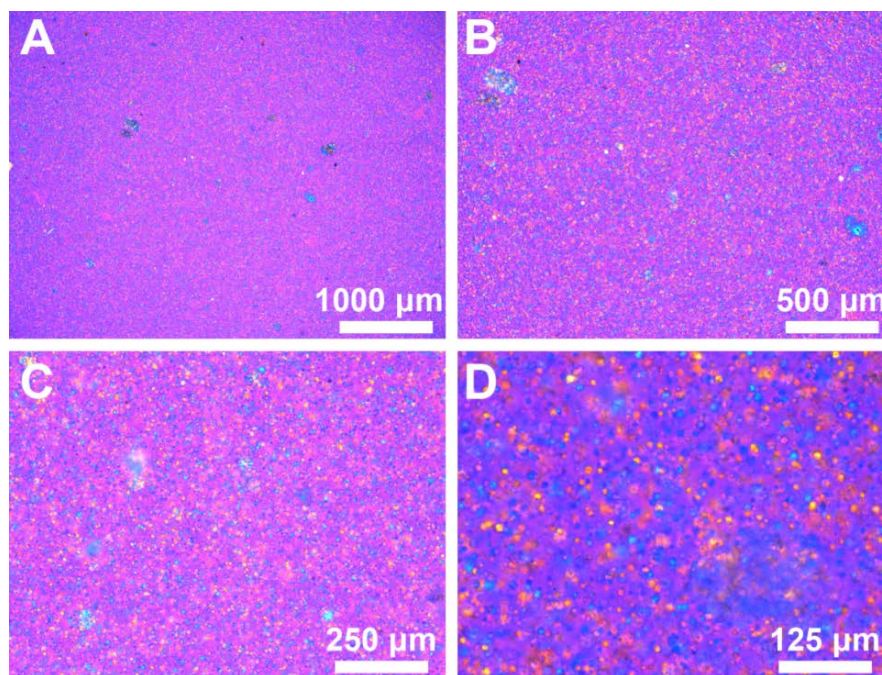


Fig. S10 Polarized optical micrograph of St@HNTs 100-20 placed under 60°C for 14 days with different magnification.

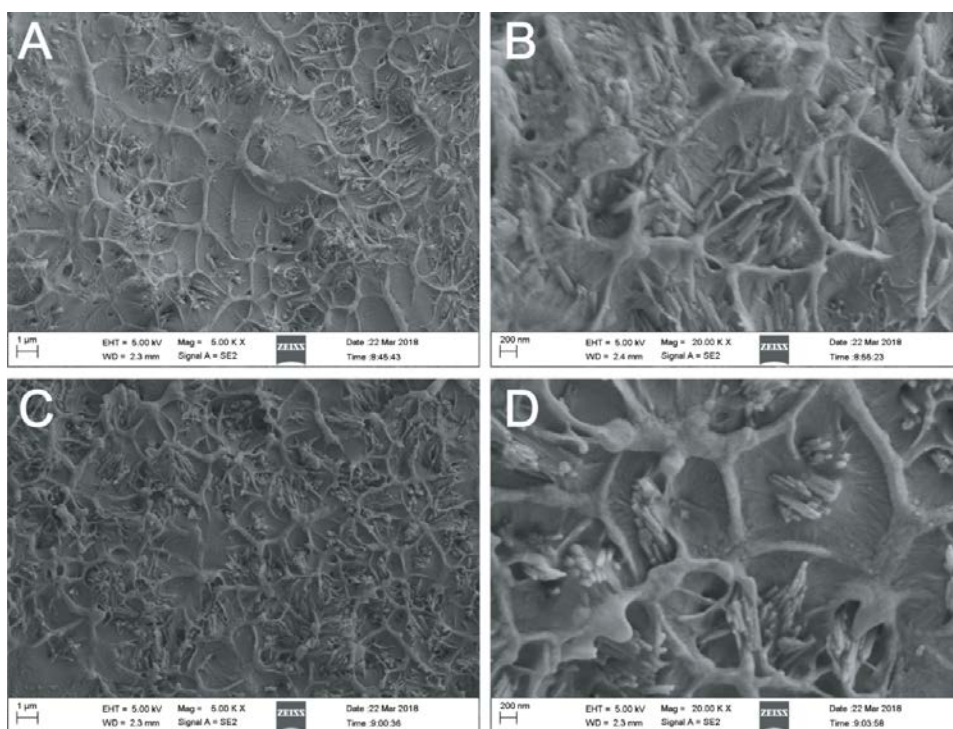


Fig. S11 SEM image of the cross section of HNTs@PS polymerized at 60°C (A, B) and polymerized at 80°C (C, D).

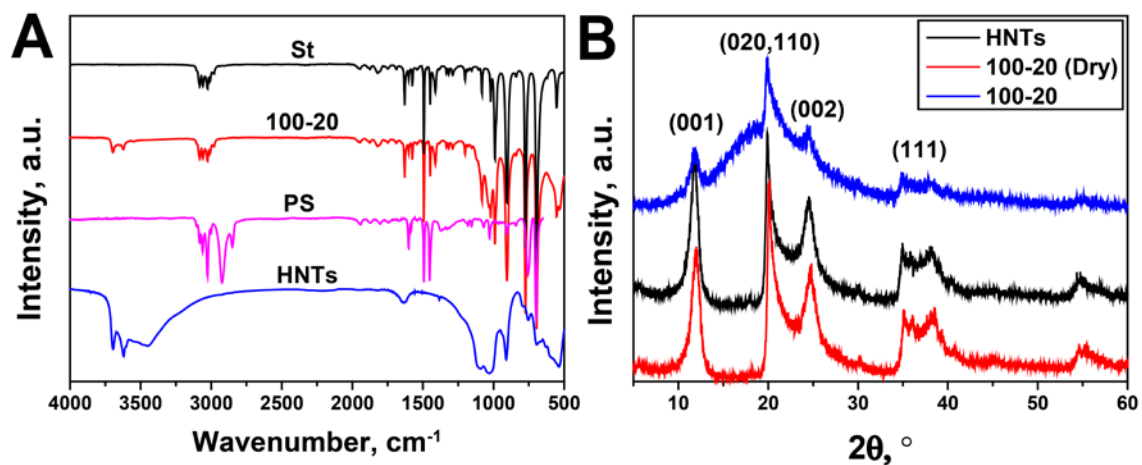


Fig. S12 FTIR spectrum (A) of St, St@HNTs 100-20, PS and HNTs; XRD pattern (B) of HNTs, powder of dry St@HNTs 100-20 and St@HNTs 100-20.

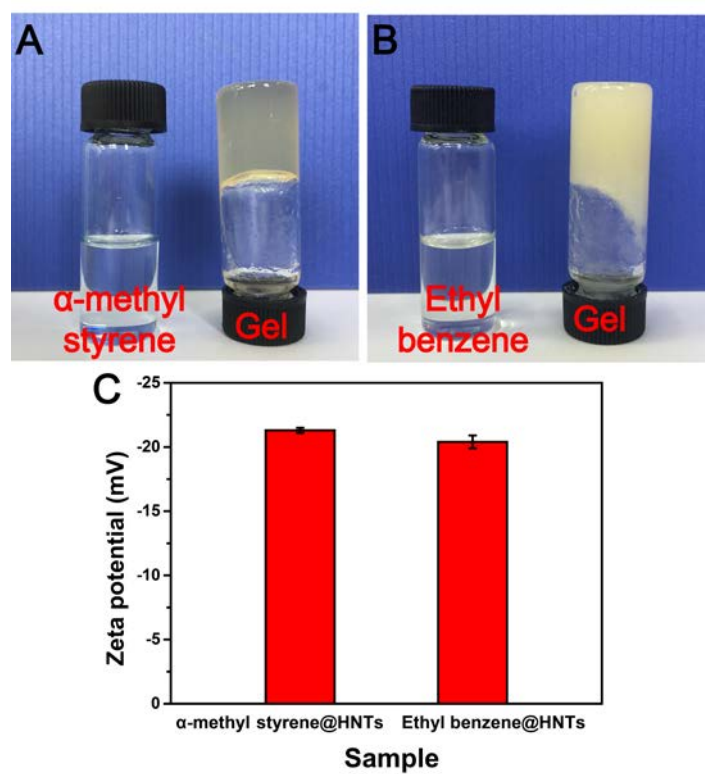


Fig. S13 The appearance of α -methyl styrene@HNTs (A) and ethyl benzene@HNTs (B); zeta potentials of α -methyl styrene@HNTs and ethyl benzene@HNTs (C).

Reference

1. M. Liu, B. Guo, Q. Zou, M. Du, D. Jia, Nanotechnology, 2008, 19(20):205709.
2. A. Alberti, M. Benaglia, M. Laus, D. Macciantelli, K. Sparnacci, Macromolecules, 2003, 36(3):736-740.